Theor Chem Acc (2010) 126:351–360
DOI 10.1007/s00214-009-0694-x

REGULAR ARTICLE

Theoretical study of the excited-state intramolecular proton transfer and rotamerism in 2,5-bis(2-hydroxyphenyl)-1,3,4-oxadiazole

Ruifa Jin · Jingping Zhang · Lizhu Hao

Received: 22 July 2009 / Accepted: 4 November 2009 / Published online: 22 November 2009
© Springer-Verlag 2009

Abstract The intramolecular proton transfer process, rotational process, and optical properties of 2,5-bis(2-hydroxyphenyl)-1,3,4-oxadiazole have been studied. The effects of solvents were considered using the polarized continuum mode. The calculated results revealed that the high energy barriers inhibit the proton transfers for bis-enol (BE) forms (BE1 and BE2) in S_0 states. The single proton transfers for BE forms in S_1 states can take place through low energy barriers and exothermicity, while the corresponding processes are not feasible in T_1 states due to endothermicity. The proton transfers for enol–keto (EK) forms (EK1 and EK2) are difficult to occur in S_0, S_1, and T_1 states because of the high energy barriers and large endothermicity. The rotational processes of both BE1 → BE2 and EK1 → EK3 are feasible in S_0 states, while difficult in S_1 and T_1 states because of the high energy barriers. The rotational process of both EK1 → EK2 and BK1 → BK2 are difficult to occur in S_0, S_1, and T_1 states. Furthermore, ^{1}EK1* in S_1 state can undergo ISC to the T_1 state PES of ^{3}EK1*, which may be the reason that the excited state intramolecular proton transfers can facilitate ISC to T_1 states and subsequently enhance the electroluminescent efficiency. The normal small Stokes shift emission can be assigned to ^{1}BE1* form. The large Stokes shift emission can be assigned to the ^{1}EK1* form, which was formed by the single proton transfer in S_1 state. In T_1 states, the ^{3}BE1* form shows phosphorescence emissions both in gas phase as well as in solutions. Our results give good supplementary explanations for experimental results at the molecular level.

Keywords Intramolecular proton transfer · Rotational process · Optical property · 2,5-Bis(2-hydroxyphenyl)-1,3,4-oxadiazole

1 Introduction

The photoinduced excited-state intramolecular proton transfer (ESIPT) phenomenon, which is observed in a wide range of organic molecules, has generated tremendous interest to the photo-physicists and photo-chemists because of the huge potential in it [1–8]. ESIPT usually occurs in molecules with functional groups linked by a hydrogen bond; the charge redistribution consequent upon excitation alters the acid–base properties of these groups, leading to proton transfer along the hydrogen bond in the tautomerization process. The ESIPT process is normally extremely fast occurring within the subpicosecond time scale which falls within the range of the period of low-frequency vibrations. Organic luminophores that undergo ESIPT are usually characterized by abnormally large fluorescence Stokes shifts (6,000–12,000 cm^{-1}) due to the reorganization of the charge distribution of the tautomerization [9, 10]. This property makes these molecules very attractive

Electronic supplementary material The online version of this article (doi:10.1007/s00214-009-0694-x) contains supplementary material, which is available to authorized users.

R. Jin · J. Zhang (✉)
Faculty of Chemistry, Northeast Normal University, 130024 Changchun, China
e-mail: zhangjingping66@yahoo.com.cn

R. Jin
Department of Chemistry, Chifeng University, 024000 Chifeng, China

L. Hao
Key Laboratory for Applied Statistics of MOE, 130024 Changchun, China

due to potential utilities in fluorescence sensors [11–13], laser dyes, organic light emitting diodes (OLEDs) [14–18], UV filters [19], and molecular switches [20, 21]. There are some theoretical investigations for ESIPT phenomena at the semi-empirical and ab initio levels [22–31].

2-(2-Hydroxyphenyl)-5-phenyl-1,3,4-oxadiazole (HOXD) and its derivatives are examples of molecular system that undergo ESIPT to yield excited keto forms from the original enol forms and emit quite strong ESIPT fluorescence [32–34]. Moreover, the triplet phosphorescence emissions of the enol forms [12, 14] raise the electroluminescent efficiency, which is the demand for electroluminescence materials of OLEDs. Furthermore, substances containing an oxadiazole fragment (both low molecular weight and polymers) are promising materials for the construction of OLEDs [35], both as electron-transporting and hole-blocking layers [36–38] and as light-emission layers [39, 40]. Doroshenko et al. [32, 33] performed experimental and theoretical studies of HOXD and its several derivatives to find the substituent effects on the fluorescence properties. Tong et al. [13] reported that HOXD and 2,5-bis(2-hydroxyphenyl)-1,3,4-oxadiazole can be used as fluorescence sensors for $H_2PO_4^-$ and F^- sensing. Gaenko et al. [34] studied three substituted HOXDs with the substituents being N,N′-dimethylamino, methoxy, or a phenyl group conducted at the ab initio level. In our previous report [41], we performed a theoretical study on O/"NH" and O/"S"-substituted derivatives of the HOXD to investigate the substituent effects on the intramolecular proton transfer, the rotational processes, and the optical properties. However, to the best of our knowledge, no detailed study of the various species of 2,5-bis(2-hydroxyphenyl)-1,3,4-oxadiazole (see Scheme 1) in their ground (S_0), first singlet excited (S_1), and the lowest triplet (T_1) states which contribute to photophysics has been reported so far to explain its absorption and emission spectra.

In this work, we reported the results of an extensive investigation of the intramolecular proton transfers and rotational processes in the S_0, S_1, and T_1 states on the different tautomers and rotamers of 2,5-bis(2-hydroxyphenyl)-1,3,4-oxadiazole to find out the nature of actual species that exist in the system under different environments. Furthermore, we studied the optical properties at the TD-DFT level and the effects of solvents with the aim to get an in-depth explanation of the experimental results. The various tautomeric and rotameric species involved in the 2,5-bis(2-hydroxyphenyl)-1,3,4-oxadiazole system and their interrelationships are shown in Scheme 1, along with the atom numbering, where *cis*–bis–enol (BE1) and *trans*–bis–enol (BE2) are denoted as BE forms; *cis*–enol–keto (EK1) and its rotamer (EK2), and *trans*–enol–keto (EK3) are denoted as EK forms; *cis*–bis–keto (BK1) and its rotamer (BK2) are denoted as BK forms.

2 Computational details

All calculations discussed in this work were carried out by the GAUSSIAN 03 package [42]. On the basis of our previous successful calculation for HOXD [41], the geometry optimizations for S_0 states were carried out using the ab initio Hartree Fock (HF) method, while the configuration interaction with single excitations (CIS) [43] method was employed to optimize the geometries for S_1 and T_1 states. All geometry optimizations were performed using the 6-31G(d) basis set. Frequency calculations at the same level were carried out for the obtained structures. All real frequencies confirmed the presence of a local minimum, while one imaginary frequency indicated the existence of a transition state. To introduce the dynamic electron correlation, single-point energy calculations for the ground and excited states have been carried out at the DFT and TD-DFT levels, respectively, with B3LYP, using the 6-31+G(d,p) basis set.

Absorption, fluorescence, and phosphorescence spectra were calculated using the TD-B3LYP/6-31+G(d,p) method based on the optimized ground and excited states geometries, respectively. To investigate the influence of solvents on the relative stability and optical properties for the various energy states of the molecular systems in polar (acetonitrile: dielectric constant 36.64) and non-polar (toluene: dielectric constant 2.379) solvents, we performed the polarized continuum model (PCM) [44, 45] calculations at the DFT and TD-DFT levels to give a comparison of the absorption and emission spectra in solution (toluene or acetonitrile) and gas phase. The natural radiative lifetimes both in gas phase and solutions were also calculated. The hybrid method (denoting as single-point calculation//optimization method), such as DFT//HF or TD-DFT//HF or TD-DFT//CIS has been proved to be an efficient approach in predicting energy parameters [46, 47] or optical properties for LED materials [40, 48–54].

Although the TD-DFT methods in general are better than CIS methods in explaining structures, energetics, and reactivities of molecules in various electronic states, the CIS methods provide acceptable approximations to give results which are quite close to the experimental data for the compounds under investigation. In our previous work [41], the geometry optimizations for the excited state of HOXD were also carried out at the TD-B3LYP/TZVP level by TURBOMOLE 5.7 [55] program suite. The optical properties were predicted at the TD-B3LYP/TZVP level based on the optimized excited states geometries. The calculated results revealed that the TD-B3LYP/TZVP method failed to provide a correct energy ordering with the available experimental result for the T_1 state. It was also found that TD-DFT method systematically underestimates the energy of charge-transfer excited states [56]. On the

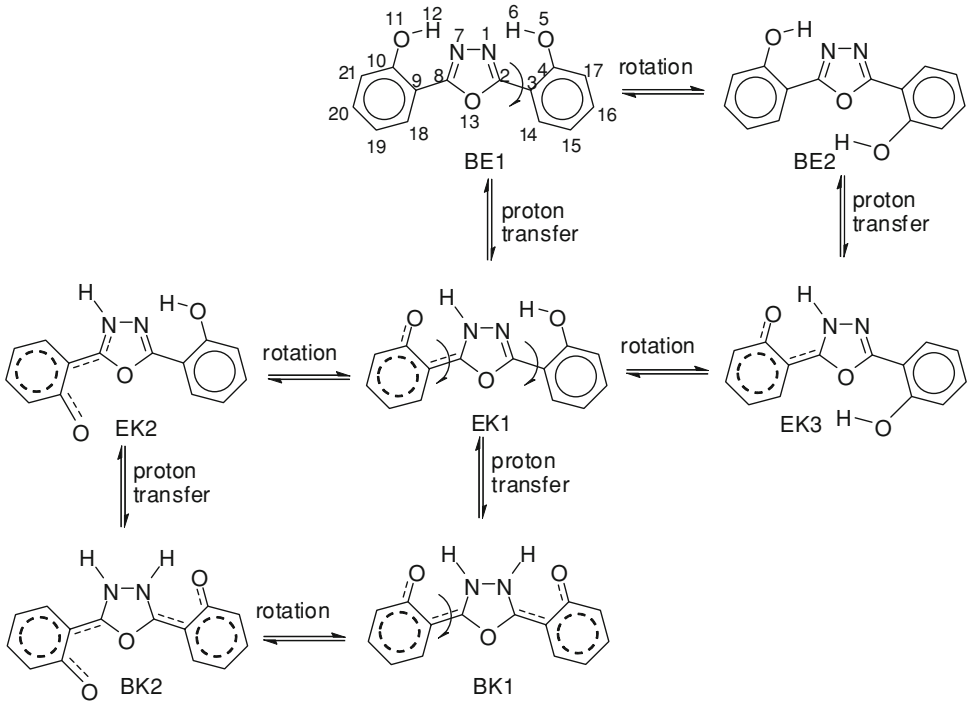

Scheme 1 The various possible tautomeric and rotameric species involved in the 2,5-bis(2-hydroxyphenyl)-1,3,4-oxadiazole and their interrelationships, along with the atom numbering

contrary, the TD-B3LYP/6-31+G(d,p)//CIS/6-31G(d) method provides a correct energy ordering with the available experimental result for the excited states (S_1 and T_1). Furthermore, the TD-B3LYP/6-31+G(d,p)//CIS/6-31G(d) method performs better in predicting the λ_{fl} and λ_{ph} for HOXD compared with the experimental data. Hence, in the present work, we perform the geometry optimizations for the tautomers and rotamers of 2,5-bis(2-hydroxyphenyl)-1,3,4-oxadiazole at the CIS/6-31G(d) level.

3 Results and discussions

3.1 Intramolecular proton transfers

3.1.1 Geometrical parameters

The main optimized geometric parameters of BE, EK, and BK forms in S_0 and S_1 states are presented in supplementary Fig. SI. Species I exhibits C_{2V} symmetry in the S_0 state, which is corroborated by the frequency calculation. The geometries of other six species were fully optimized without any symmetry constraints. The origin of the geometric difference introduced by excitation can be explained, at least in qualitative terms, by analyzing the change in the bonding character of the orbital involved in the electronic transition for each pair of bonded atoms [57]. It is useful to examine the frontier molecular orbitals (FMOs) of the compounds under investigation. The qualitative molecular orbital representations of the highest occupied molecular orbitals (HOMOs) and the lowest unoccupied molecular orbitals (LUMOs) for the seven species in S_0 states are shown in supplementary Fig. SII. When the HOMO → LUMO transition involves the loss of the bonding character of a bond (or the gain of anti-bonding character), the bond concerned is lengthened and vice versa. In all cases, both the HOMO and LUMO have π symmetry. The $S_0 \rightarrow S_1$ excitation process can be mainly assigned to HOMO → LUMO transition, which corresponds to a $\pi \rightarrow \pi^*$ excited singlet state. We compared the different geometrical parameters involved in proton transfers processes. The structural parameters displayed in supplementary Fig. SI reveal that the $S_0 \rightarrow S_1$ excitation affects the π densities of the C–C bonds constituting the chelate ring (HOCCCN) (for atoms labeling, see Scheme 1). For BE1 → BE1*, both the C2–C3 and C8–C9 inter-ring bonds are shortened by 0.06 Å, while the C3–C4, C9–C10, N1–C2, and N7–C8 bonds are elongated by 0.04, 0.04, 0.06, and 0.06 Å, respectively. For BE2 → BE2*, the C2–C3 and C8–C9 inter-ring bonds are all shortened by 0.04 Å, while the C3–C4, C9–C10, N1–C2, and N7–C8 bonds are elongated by 0.02, 0.02, 0.03, and 0.03 Å, respectively. Similar phenomena are found for EK forms, except for a lengthening of the C8–C9 bond slightly. On the contrary, the C2–C3 and C8–C9 inter-ring bonds for $S_0 \rightarrow S_1$ excitation of BK forms are elongated. The C9–C10 and N7–C8 bonds of BK1 are elongated while the C9–C10 and N1–C2 bonds of BK2 are shortened. Changes in the bond lengths in the excited states with respect to their ground state geometries can be ascribed to the changes in bonding character.

3.1.2 *Electron density redistribution and the changes in acid–base properties of the groups*

It is well known that the main driving force of ESIPT reaction is the increase of the excited state acidity of the proton donor moiety and the excited state basicity of the proton acceptor group. Such changes in protolytic properties can be ascribed to the excited state redistribution of electron density in the molecules capable of the proton phototransfer reaction [58–60]. Figures 1 and 2 show the electrostatic surface potentials in S_0 and S_1 states for BE (BE1 and BE2) and EK (EK1, EK2, and EK3) forms, respectively. The electrostatic surface potentials for BK forms in S_0 and S_1 states are presented in supplementary Fig. SIII. Inspection of Fig. 1 reveals clearly that the excitations of the electrons from S_0 to S_1 states lead to the electronic densities flow mainly from the two phenolic rings to the heterocycle ring for BE1 while from the one (left) phenolic and oxadiazole rings to another (right) phenolic ring for BE2. The BE forms feature an inverse electron density distributions in S_0 and S_1 states for the locations of the oxygen atoms of hydroxy groups and nitrogen atoms of oxadiazole rings. Such a pronounced difference in the electrostatic surface potentials can trigger a modification of the acid–base properties of the groups. In terms of acid–base interactions this results in an increase of the acidity of the hydroxy group (the proton donor), and, correspondingly, an increase in the basicity of the oxadiazole ring (the proton acceptor) [37, 38]. The increase in the acidity and basicity of the hydroxy group and oxadiazole ring could also be predicted from the changes of charges on the hydroxylic oxygen atoms and the nitrogen atoms of oxadiazole ring, Δq_O and Δq_N [37]. The values of Δq_{O5}, Δq_{O11}, Δq_{N1}, and Δq_{N7} for BE1 are 0.013, 0.013, −0.004, and −0.004, the corresponding values for BE2 are 0.073, 0.012, −0.08, and −0.146, respectively (see Table SI in supplementary). Such coordinated changes of acid–base properties of the groups, connected to one another by an intramolecular hydrogen bond, constitute the driving force of the excited state proton transfer reaction. The increases of the acidities of the hydroxy groups and the basicities of the oxadizole rings for the BE forms favor the proton transfers from ^{1}BE* to ^{1}EK* forms in S_1 states. There will be the increase in the acidities for the protonated heterocycles and basicities of the ketonic rings after the relaxation of the EK forms from S_1 to S_0 states through fluorescent emissions. Those favor the reverse proton transfers from EK forms to the starting BE forms in S_0 states to finish the cyclic four-level photophysical scheme (BE → ^{1}BE* → ^{1}EK* → EK → BE).

For EK forms (EK1, EK2, and EK3), the electronic densities flow mainly from the phenolic and protonated heterocycle rings to ketonic rings, as shown in Fig. 2. One can find that the changes in the electronic densities and charges on the hydroxylic oxygen atoms and the nitrogen atoms of oxadiazole rings upon excitations increase the basicity of nitrogen in oxadiazole rings, while decrease the acidities of the hydroxy groups of phenolic rings for the ^{1}EK* forms (see Table SI in supplementary), which hinder the proton transfers from ^{1}EK* to ^{1}BK* forms in S_1 states. Thus, it can be expected that the processes of the second proton transfers from ^{1}EK* to ^{1}BK* forms are more difficult than the processes of the first proton transfers from ^{1}BE* to ^{1}EK* forms in S_1 states.

In the case of BK forms, the trends of electronic densities flow for BK1 and BK2 are similar to those in BE2 and EK1, respectively, as shown in supplementary Fig. SIII.

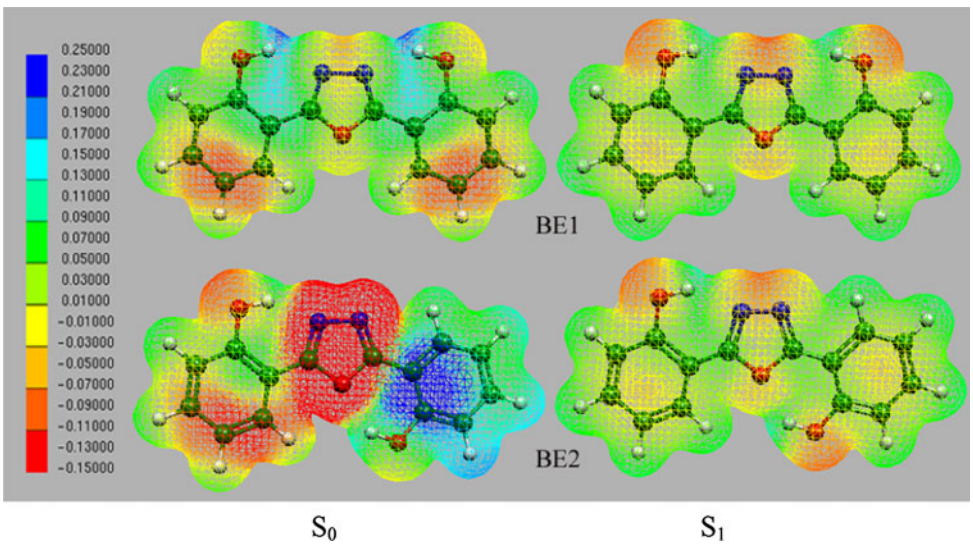

Fig. 1 Electrostatic surface potentials in S_0 and S_1 states for BE. Regions of higher electron density are shown in *red* and of lower electron density in *blue* (values in atomic units)

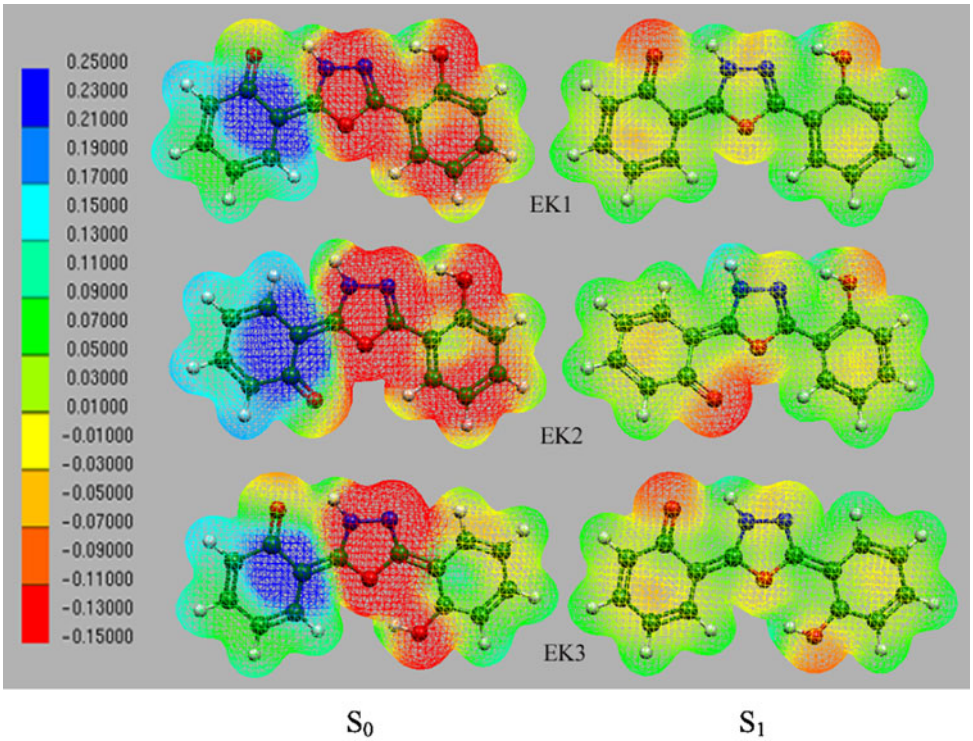

Fig. 2 Electrostatic surface potentials in S_0 and S_1 states for EK. Regions of higher electron density are shown in *red* and of lower electron density in *blue* (values in atomic units)

3.1.3 Energy parameters

Figures 3 and 4 present relative energies (in kcal/mol) for proton transfers and rotational processes in S_0 and S_1 states in the gas phase. The corresponding values in T_1 states are presented in supplementary Fig. SIV. The results displayed in Fig. 3 show that the BE and EK forms are much more stable than EK and BK forms, respectively, which are ascribed to the existence of two aromatic phenol rings in BE forms and one aromatic phenol ring in EK forms, while no aromatic phenol ring in the BK forms. It is worth noting that the proton transfer processes in S_0 states involve high direct energy barrier ($\Delta E_d^{\#}$) and relative energies (ΔE) (energies differences between products and reactants) because of the loss of aromaticity along these processes from BE to EK and EK to BK forms. Furthermore, the slightly negative values of reverse energy barrier ($\Delta E_r^{\#}$) suggest that B3LYP method slightly underestimates the energy barriers of the proton transfers processes. It was also recently reported that the B3LYP method provides negative energy barriers for radical addition reaction [61]. Within the limits of the method, the large endothermicity and high $\Delta E_d^{\#}$ impose a restriction on the occurrence of the proton transfer in S_0 state for each species. However, the reverse proton transfer will occur easily through a very low energy barrier or a barrierless process.

Comparing the results shown in Figs. 3 with 4, one can find that the endothermic proton transfer processes from BE to EK in S_0 states become exothermic in S_1 states. The $\Delta E_d^{\#}$ values of ^{1}BE1* → ^{1}EK1* and ^{1}BE2* → ^{1}EK3* in S_1 states are lower than those in S_0 states by 11.9 and 13.9 kcal/mol, respectively. However, for the second proton transfer processes, as expected, the decrease the acidities of the hydroxy groups of phenolic rings for the ^{1}EK* forms upon excitations hinder the proton transfers from ^{1}EK* to ^{1}BK* forms in S_1 states. The ΔE values of both ^{1}EK1* → ^{1}BK1* and ^{1}EK2* → ^{1}BK2* in S_1 states exhibit high endothermicities as in S_0 states. The corresponding $\Delta E_d^{\#}$ values are similar to those in S_0 states. It suggests that both ^{1}EK1* → ^{1}BK1* and ^{1}EK2* → ^{1}BK2* are difficult to take place in S_1 states. The general observations from Fig. 4 suggest the ESIPT processes can take place easily through lower energy barriers in S_1 states for ^{1}BE* forms (^{1}BE1* and ^{1}BE2*), while the ESIPT processes of ^{1}EK* forms (^{1}EK1* and ^{1}EK2*) are difficult to occur in S_1 states because of high values of $\Delta E_d^{\#}$ and endothermicities.

In T_1 states, the ΔE values of ^{3}BE1* → ^{3}EK1* and ^{3}BE2* → ^{3}EK3* are 0.4 and 1.5 kcal/mol, which are lower than those in S_0 states by 15.3 and 18.1 kcal/mol, respectively. The corresponding $\Delta E_d^{\#}$ values are 9.2 and 8.7 kcal/mol, and the $\Delta E_r^{\#}$ values are 8.8 and 7.2 kcal/mol. For ^{3}EK1* → ^{3}BK1* and ^{3}EK2* → ^{3}BK2* processes, the $\Delta E_d^{\#}$ values are similar to those in S_0 and S_1 states and the ΔE values exhibit high endothermicities (see Fig. SIV in supplementary). Therefore, the proton transfer from BE to EK and EK to BK processes are difficult to occur, while the reverse proton transfer processes EK to BK can take place in T_1 states.

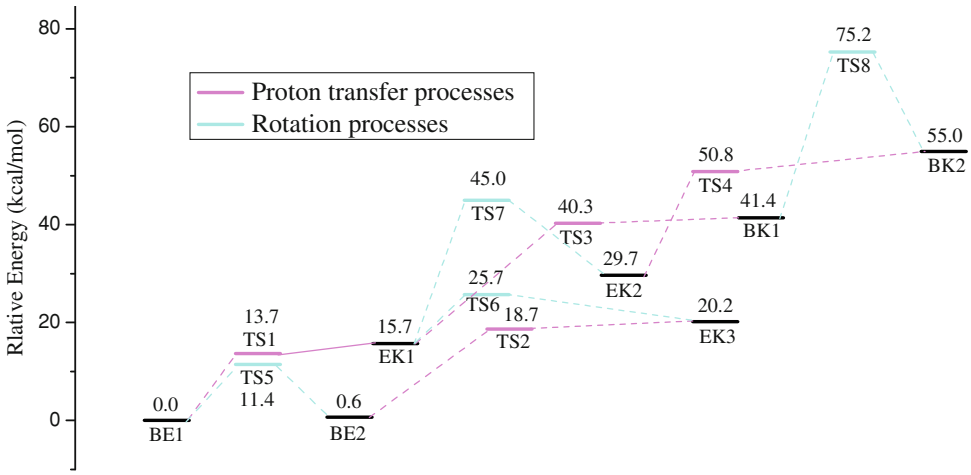

Fig. 3 Relative energies (in kcal/mol) for proton transfers (*light magenta*) and rotational (*light cyan*) processes in S_0 states in the gas phase. TS1-4 are donated the transition states of proton transfers processes of BE1 → EK1, BE2 → EK3, EK1 → BK1, and EK2 → BK2, respectively. TS5-8 are donated the transition states of rotational processes of BE1 → BK2, EK1 → EK3, EK1 → EK2, and BK1 → BK2, respectively

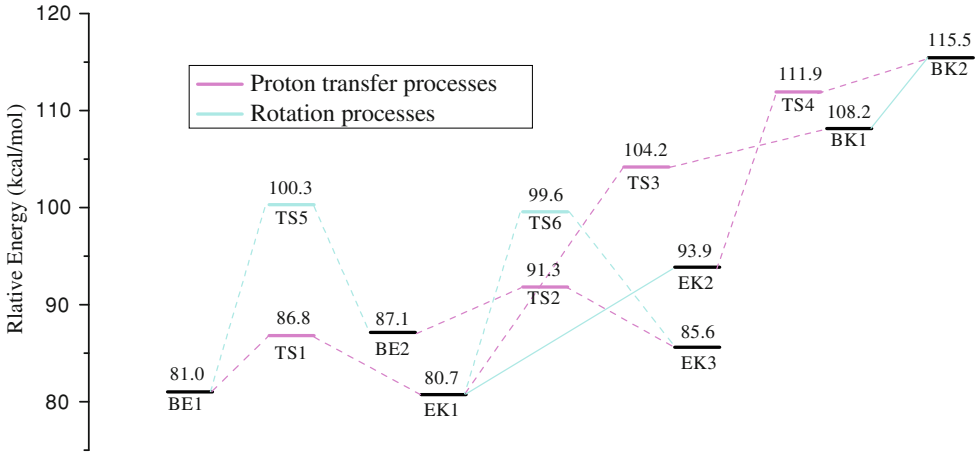

Fig. 4 Relative energies (in kcal/mol) for proton transfers (*light magenta*) and rotational (*light cyan*) processes in S_1 states in the gas phase. TS1-4 are donated the transition states of proton transfer processes of ^{1}BE1* → ^{1}EK1*, ^{1}BE2* → ^{1}EK3*, ^{1}EK1* → ^{1}BK1*, and ^{1}EK2* → ^{1}BK2*, respectively. TS5-6 are donated the transition states of rotational processes of ^{1}BE1* → ^{1}BK2* and ^{1}EK1* → ^{1}EK3*, respectively

3.2 Rotational processes

Table 1 presents the relative energy and dipole moment of each species in S_0, S_1, and T_1 states in gas phase as well as solvated (in toluene and acetonitrile) conditions. As shown in Table 1, BE1/BK1 is more stable than BE2/BK2, respectively, and EK1 is the most stable among EK forms in S_0 state. Furthermore, the $\Delta E_d^{\#}$ values of BE1 → BE2, EK1 → EK3, EK1 → EK2, and BK1 → BK2 in S_0 states are 11.4, 10.0, 29.3, and 33.8 kcal/mol, respectively (see Fig. 3). It suggests that the rotational processes of BE1 → BE2 and EK1 → EK3 can occur, while EK1 → EK2 and BK1 → BK2 are difficult to occur in S_0 states.

In S_1 and T_1 states, the $\Delta E_d^{\#}$, $\Delta E_r^{\#}$, and ΔE values of BE1* → BE2* and EK1* → EK3* are larger than those in S_0 states. The $\Delta E_d^{\#}$ values of BE1* → BE2* in S_1 and T_1 states are 19.3 and 16.8 kcal/mol, and the corresponding values of EK1* → EK3* are 18.9 and 10.4 kcal/mol, respectively. For EK1* → EK2* and BK1* → BK2*, the high energy barriers of the rotational processes in S_0 states become high endothermic barrierless processes in S_1 states. The $\Delta E_d^{\#}$ and ΔE values of ^{3}EK1* → ^{3}EK2* and ^{3}BK1* → ^{3}BK2* in T_1 states are lower than those in S_0 states and are larger than those of BE1* → BE2* and EK1* → EK3* in T_1 states, respectively. Hence, the high energy barriers and/or endothermic processes inhibit the rotational processes in S_1 and T_1 states.

On the basis of the results described above, one can conclude that the rotational processes of both BE1 → BE2 and EK1 → EK3 are feasible in S_0 states, while difficult in S_1 and T_1 states because of the high energy barriers. The rotational process of both EK1 → EK2 and BK1 → BK2 are difficult to occur in S_0, S_1, and T_1 states.

3.3 Potential energy surfaces crossing

With the aim to explore the mechanism for the high endothermic barrierless rotational processes EK1 → EK2 and BK1 → BK2 in S_1 states, we performed the reaction paths and energy profiles of these rotational processes in their S_0, S_1, and T_1 states. One internal degree of freedom (a dihedral angle N_7–C_8–C_9–C_{10}; see Scheme 1) as the driving coordinate was selected and the other internal coordinates were

Table 1 Relative energies E (in kcal/mol) of different species in gas phase as well as solvated (in toluene and acetonitrile) conditions in S_0, S_1, and T_1 states and dipole moments μ (in debye) of different species in S_0, S_1, and T_1 states

Species	S_0				S_1				T_1			
	E			μ	E			μ	E			μ
	Gas	$C_6H_5CH_3$	CH_3CN		Gas	$C_6H_5CH_3$	CH_3CN		Gas	$C_6H_5CH_3$	CH_3CN	
BE1	0	−3.9	−9.0	3.8	81.0	74.8	71.1	3.7	58.2	54.7	50.0	3.9
BE2	0.6	−3.8	−9.7	2.7	87.1	80.2	75.8	2.6	61.4	57.5	52.4	2.7
EK1	15.7	9.8	2.26	4.8	80.7	75.9	70.8	5.1	58.6	54.7	49.7	4.6
EK2	29.7	21.6	10.6	4.0	93.8	86.4	77.7	4.0	64.3	60.2	53.4	3.2
EK3	20.2	14.2	6.6	4.4	85.6	80.3	75.0	4.8	62.9	58.9	53.7	4.2
BK1	41.4	34.1	24.6	3.4	108.2	99.9	91.7	3.6	79.2	73.0	65.2	3.7
BK2	55.0	45.8	33.7	3.8	115.5	106.7	95.9	3.7	81.2	77.5	68.3	3.5

optimized in S_0 states at the HF/6-31G(d) level. On the basis of the optimized structures, the single-point energy calculations have been carried out at the B3LYP/6-31+G(d,p) and TD-B3LYP/6-31+G(d,P) levels to obtain the S_0, S_1, and T_1 states energy values for each of the rotational conformers (rotamers), respectively. This method provides acceptable approximations to give results, which are quite close to the experimental findings [27, 62]. Figure 5 shows the simulated energy profiles of the rotational processes of EK1 → EK2 in S_0, S_1, and T_1 states. Inspection of Fig. 5 reveals clearly that it contains a potential energy surface (PES) crossing (geometries where multiple electronic states are exactly degenerate) between S_1 and T_1 states, which is located in the zone corresponding to the position that the ketonic ring is almost perfectly perpendicular to the protonated heterocycle plane (e.g., torsion angle $\theta_{N7–C8–C9–C10} = 90°$). The investigation of a mechanism of a photochemical reaction involves a characterization of the regions where the potential energy surface (PES) crossings occur. These regions are where fast internal conversion or intersystem crossing (ISC) are expected to take place

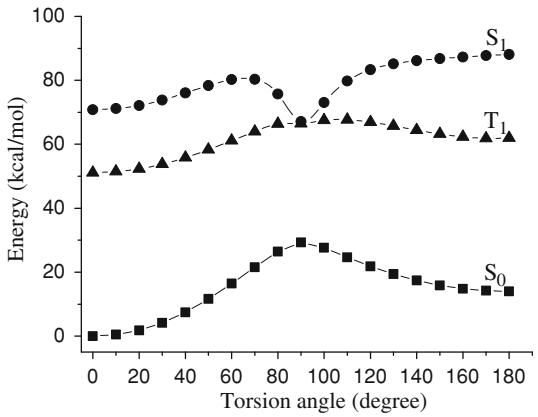

Fig. 5 Plot of total energy as a function of torsion angle (N_7–C_8–C_9–C_{10}) for rotational process of EK1 → EK2 in the S_0, S_1, and T_1 states

[63–65]. For the energy values of ^{1}EK1* and ^{1}EK2* are higher than those of ^{3}EK1* and ^{3}EK2* by ca. 22 and 30 kcal/mol, respectively, the ^{1}EK1* in rotational process of ^{1}EK1* → ^{1}EK2* in S_1 state could undergo ISC to the T_1 state PES of ^{3}EK1* and ^{3}EK2*, particularly to PES of ^{3}EK1*. This may be the reason that the ESIPT can facilitate ISC and subsequent enhancement of T_1 state excitation. This phenomenon can be observed in the case of ^{1}BK1* → ^{1}BK2* (see Fig. SV in supplementary).

3.4 Electronic transition

We summarized the calculated results of vertical excitation energies along with available experimental data in Table 2. In gas phase, the absorptions ($\lambda_{abs} = 313$ nm) correspond to the excitation of BE forms (BE1 and BE2) because of they being the most abundant and stable species in S_0 state (see Table 1). After the photoexcitation of the BE forms (BE1 and BE2) to the lowest excited singlet states ^{1}BE* forms (^{1}BE1* and ^{1}BE2*), the ^{1}BE1* and ^{1}BE2* forms can transfer their protons of the phenolic rings to the nitrogen atom (N_1) of oxadiazole rings and form the ^{1}EK1* and ^{1}EK3* forms, respectively. Hence, the short-wavelength emission can be assigned to the emissions of ^{1}BE1* and ^{1}BE2* ($\lambda_{fl} = 362$ nm) and the long-wavelength emission band characterized by high Stokes shift value is attributed to the emission of ^{1}EK1* and ^{1}EK2* forms. For ^{1}EK1* is more stable than ^{1}EK2* by 7 kcal/mol and its λ_{fl} value is similar to that of ^{1}EK2*, we give the λ_{fl} values of ^{1}EK1* in gas phase and solutions as representatives of the long-wavelength emissions in Table 2. In general, larger oscillator strength corresponds to larger experimental absorption coefficient or stronger fluorescence intensity. From Table 2 one can find that the f values of absorptions for BE1 and BE2 forms are larger than 0.5. The f values of emissions for ^{1}BE1* are larger than 0.77, while the corresponding f values of ^{1}EK1* are larger than 0.2. It suggests that the BE1, BE2, and EK1 show the intensive spectrum in gas

Table 2 Calculated absorption (λ_{abs}), fluorescence (λ_{fl}), and phosphorescence (λ_{ph}) wavelengths (in nm) and their oscillator strengths (in the parentheses) in gas phase as well as solvated (in toluene and acetonitrile) conditions, along with available experimental data of 2,5-bis(2-hydroxyphenyl)-1,3,4-oxadiazole

	Gas	Toluene	Acetonitrile
λ_{abs}	313 (0.52), 310 (0.50)	317 (0.67), 315 (0.65)	313 (0.64), 312 (0.60)
λ_{fl}	362 (0.77), 455(0.20)	374 (0.94), 444 (0.33)	368 (0.91), 422 (0.35)
λ_{ph}	517	513	508
Exp[a]		365[b], 500[b]	365[c], 436[c]

[a] Experimental results were taken from Ref. [13]

[b] The values are the experimental λ_{fl} in toluene

[c] The values are the experimental λ_{fl} in acetonitrile

phase as well as solvated (in toluene and acetonitrile) conditions. Furthermore, ^{1}EK1* can also transit to ^{3}EK1* through the ISC. For the molecules with ESIPT property, it was found that the ESIPT facilitates the ISC [66]. Consequently, phosphorescence emissions of ^{3}EK1* should be observed. However, ^{3}EK1* may take place subsequently the reverse proton transfers to form ^{3}BE1* forms in T_1 states because of the low energy barrier and exothermicity (see Fig. SIV in supplementary). Hence, phosphorescence emissions correspond to the ^{3}BE1*.

The radiative lifetimes of seven species have been estimated by using the Strickler and Berg relationship [67, 68]

$$\tau = \frac{1}{k_r} = \frac{E_{S0-S1}}{0.667 n^2 f E^3_{S1-S0}}$$

Here, k_r is the radiative rate constant, n is the refractive index of the solvent used in the experiments (the n values of toluene and acetonitrile are 1.4941 and 1.3441, respectively), f is the oscillator strength, E_{S1-S0} and E_{S0-S1} are the vertical fluorescence and absorption transition energies, respectively, in cm^{-1} units. The results are listed in supplementary Table SII. According to our calculations, we can draw a qualitative conclusion that the fluorescence emitting times of ^{1}EK* forms are longer than those of ^{1}BE* forms both in gas phase and solution. It indicates that deactivation process is competitive with ISC. Before fluorescence emitted, the excited ^{1}EK1* forms execute quick ISC when all the other conditions cooperate. Subsequently, the ^{3}EK1* can take place in the reverse proton transfers to form ^{3}BE1*. As a result, the ^{3}BE1* can emit phosphorescence, which can enhance the electroluminescent efficiency that is the demanding for electroluminescence materials of OLEDs in flat panel display technologies.

3.5 Effects of solvents

The photophysical properties of 2,5-bis(2-hydroxyphenyl)-1,3,4-oxadiazole has been reported to be very sensitive to the nature of the solvent, and large differences have been observed in polar and non-polar solvents [13]. On the basis of their optimized structures in gas phase, we also calculated the ΔE, $\Delta E^{\#}_d$, and $\Delta E^{\#}_r$ for the proton transfers and rotational processes in toluene and acetonitrile solutions (see Figs. SVI–SXI in supplementary).

For the rotational processes, the ΔE, $\Delta E^{\#}_d$, and $\Delta E^{\#}_r$ values of BE1 → BE2, EK1 → EK2, EK1 → EK3, and BK1 → BK2 in S_0, S_1, and T_1 states both in toluene and acetonitrile solutions are decreased compared with those in gas phase, respectively. Furthermore, the ΔE, $\Delta E^{\#}_d$, and $\Delta E^{\#}_r$ values in toluene are larger than those in acetonitrile. Therefore, all the rotational processes will take place easier in toluene and acetonitrile solutions than those in the gas phase; particularly in acetonitrile solution (see Figs. SVI–SXI in supplementary). For the proton transfers processes, the ΔE and $\Delta E^{\#}_d$ values of the ^{1}BE* → ^{1}EK* both in toluene and acetonitrile solutions are increased slightly compared with those in gas phase (deviation within 2.5 kcal/mol), while the corresponding values of the second proton transfers processes ^{1}EK* → ^{1}BK* both in toluene and acetonitrile solutions are decreased slightly compared with those in gas phase, with the maximum deviation being <7 kcal/mol. This suggests that ^{1}EK2* → ^{1}BK2* and ^{1}EK1* → ^{1}BK1* processes in S_1 states can hardly take place in toluene and acetonitrile solutions as those in gas phase.

The calculated dipole moments show that the EK forms are more polar than those of BE and BK forms both in S_0 and S_1 states (see Table 1). It appears to have a great effect on the polarities of ^{1}EK* forms than on those of ^{1}BE* and ^{1}BK* forms in S_1 states. Thus, ^{1}EK* forms are solvated more strongly than those of other forms in S_1 states. Therefore, it is difficult for the second proton to transfer from oxygen atom of the right phenolic ring to nitrogen atom of oxadiazole ring for ^{1}EK1* and ^{1}EK2* (^{1}EK1* → ^{1}BK1* and ^{1}EK2* → ^{1}BK2*) in polar solvents. The species ^{1}EK1* has the largest value of dipole moment (5.06 D) and lower energy in S_1 state among the ^{1}EK* forms in this study. Therefore, the species ^{1}EK1* can be solvated strongly by acetonitrile and are the most

abundant and stable species in S_1 state among the ^{1}EK* forms.

Therefore, the short-wavelength bands with normal small Stokes shift values both in gas phase and solvents can be assigned to the emission of BE form ^{1}BE1*. The long-wavelength bands are characterized by high Stokes shift values and may be attributed to the emission of the ^{1}EK* form ^{1}EK1*, which formed by the proton transfers in S_1 state. The fluorescence spectra of other ^{1}EK* forms (^{1}EK2* and ^{1}EK3*) may overlap with that of ^{1}EK1* substantially. The ^{3}BE1* can emit phosphorescence.

On the basis of their optimized structures in S_0, S_1, and T_1 states in gas phase, we predict the absorption and emission spectra in toluene and acetonitrile solutions taking into account solute–solvent effects at the PCM-TD-B3LYP/6-31+G(d,p) level (see Table 2). The results displayed in Table 2 reveal that there is drastic displacement of λ_{abs}, λ_{fl}, and λ_{ph} when solvent effects are taken into account for high dipole moments species (EK1). Furthermore, the TD-B3LYP method provides very good predictions for the short-wavelength emissions of ^{1}BE1* both in toluene and acetonitrile solutions. The results are all in excellent agreement with experimental results [13], with the maximum deviation being <9 and 3 nm, respectively. However, for the long-wavelength emission of ^{1}EK1*, the TD-B3LYP calculations show poor performances for predicting the λ_{fl} for ^{1}EK1*. It is known that standard TD-DFT calculations show poor performances for charge-transfer electronic transitions [69, 70]. Other researchers [71, 72] have noted that the TD-B3LYP method does not correctly describe the delocalized excited states with charge-transfer component. The poor performance of the TD-B3LYP approach may be due to insufficient flexibility in the functional. More exhaustive investigations are needed before firm conclusions can be drawn.

4 Conclusions

In this article, we have studied the ground and excited-state behavior of the 2,5-bis(2-hydroxyphenyl)-1,3,4-oxadiazole in polar and non-polar solvents. The following conclusions can be drawn. (1) The rotational process of BE1 → BE2 and EK1 → EK3 are feasible in S_0 states while difficult in S_1 and T_1 states because of the high energy barriers. The rotational processes of ^{1}EK1* → ^{1}EK2* and ^{1}BK1* → ^{1}BK2* are difficult to occur in S_0, S_1, and T_1 states. Furthermore, ^{1}EK1* in S_1 states can undergo ISC to the T_1 state PES of ^{3}EK1*, which can take place in the reverse proton transfers to form ^{3}BE1*. Consequently, ^{3}BE1* can emit phosphorescence, which can enhance the electroluminescent efficiency. (2) High energy barriers inhibit the proton transfers for BE to EK in S_0 states. The proton transfers for BE to EK in S_1 states can take place through low energy barriers and exothermicity, while the corresponding processes are not feasible in T_1 states due to endothermicity. The proton transfers for EK to BK are difficult to occur in all electronic states because of the large endothermicity and high energy barriers. (3) The normal small Stokes shift emissions both in gas phase and solvents (non-polar and polar) can be assigned to ^{1}BE1* form. The large Stokes shift emissions in gas phase and solvents can be assigned to the ^{1}EK1* form, which was formed by the single proton transfer in S_1 state. (4) In T_1 states, ^{3}BE1* shows emission phosphorescence both in gas phase as well as in solutions.

Acknowledgments Financial supports from the NSFC (Nos. 50873020, 20773022), the NCET-06-0321, the JLSDP (20082212), and the NENU-STB-07-007 are gratefully acknowledged.

References

1. Park S, Seo J, Kim SH, Park SY (2008) Adv Funct Mater 18:726
2. Nosenko Y, Wiosna-Sałyga G, Kunitski M, Petkova I, Singh A, Buma WJ, Thummel RP, Brutschy B, Waluk J (2008) Angew Chem Int Ed Engl 47:6037
3. Ding L, Chen X, Fang W-H (2009) Org Lett 11:1495
4. Barbatti M, Aquino AJA, Lischka H, Schriever C, Lochbrunner S, Riedle E (2009) Phys Chem Chem Phys 11:1406
5. Chen C-L, Lin C-W, Hsieh C-C, Lai C-H, Lee G-H, Wang C-C, Chou P-T (2009) J Phys Chem A 113:205
6. Wu Y, Peng X, Fan J, Gao S, Tian M, Zhao J, Sun S (2007) J Org Chem 72:62
7. Qian Y, Li S, Zhang G, Wang Q, Wang S, Xu H, Li C, Li Y, Yang G (2007) J Phys Chem B 111:5861
8. Sakota K, Inoue N, Komoto Y, Sekiya H (2007) J Phys Chem A 111:4596
9. Douhal A, Lahmani F, Zewail AH (1996) Chem Phys 207:477
10. Douhal A, Lahmani F, Zehnacker-Rentien A (1993) Chem Phys 178:493
11. Sytnik A, Kasha M (1994) Proc Natl Acad Sci USA 91:8627
12. Liang F, Wang L, Ma D, Jing X, Wang F (2002) Appl Phys Lett 81:4
13. Tong H, Zhou G, Wang L, Jing X, Wang F, Zhang J (2003) Tetrahedron Lett 44:131
14. Yi Y, Zhu L, Shuai Z (2008) Macromol Theory Simul 17:12
15. Rogach AL, Gaponik N, Lupton JM, Bertoni C, Gallardo DE, Dunn S, Li Pira N, Paderi M, Repetto P, Romanov SG, Dwyer CO, Sotomayor Torres CM, Eychmuller A (2008) Angew Chem Int Ed Engl 47:6538
16. Hlawacek G, Puschnig P, Frank P, Winkler A, Ambrosch-Drax C, Teichert C (2008) Science 321:108
17. Ki W, Li J (2008) J Am Chem Soc 130:8114
18. Namai H, Ikeda H, Hoshi Y, Kato N, Morishita Y, Mizuno K (2007) J Am Chem Soc 129:9032
19. Keck J, Kramer HEA, Port H, Hirsch T, Fischer P, Rytz G (1996) J Phys Chem 100:14468
20. Douhal A, Sastre R (1994) Chem Phys Lett 219:91
21. Irie M (2000) Chem Rev 100:1683 (special issue)
22. Purkayastha P, Chattopadhyay N (2002) J Mol Struct 604:87
23. Coe JD, Martinez TJ (2006) J Phys Chem A 110:618
24. Coe JD, Levine BG, Martinez TJ (2007) J Phys Chem A 111:11302

25. Sobolewski AL, Domcke W (1999) Phys Chem Chem Phys 1:3065
26. Coe J, Martinez TJ (2005) J Am Chem Soc 127:4560
27. Doltsinis NL (2004) Mol Phys 102:499
28. Wu Y, Batista V (2006) J Chem Phys 124:224305
29. Guallar V, Batista VS, Miller WH (2000) J Chem Phys 113:9510
30. Sobolewski AL, Domcke W (1994) Chem Phys 184:115
31. Nagaoka S, Nakamura A, Nagashima U (2002) J Photoch Photobio 154:23
32. Doroshenko AO, Posokhov EA, Verezubova AA, Ptyagina LM (2000) J Phys Org Chem 13:253
33. Doroshenko AO, Posokhov EA, Verezubova AA, Ptyagina LM, Skripkina VT, Shershukov VM (2002) Photochem Photobiol Sci 1:92
34. Gaenko AV, Devarajan A, Tselinskii IV, Ryde U (2006) J Phys Chem A 110:7935
35. Tamoto N, Adachi C, Nagai K (1997) Chem Mater 9:1077
36. Uchida M, Adachi C, Koyama T, Taniguchi Y (1999) J Appl Phys 86:1680
37. Wang JF, Jabbour GE, Mash EA, Anderson J, Zhang Y, Lee PA, Armstrong NR, Peyghambarian N, Kippelen B (1999) Adv Mater 11:1266
38. Kido J, Hayase H, Hongawa K, Nagai K, Okuyama K (1994) Appl Phys Lett 65:2124
39. Antoniadis H, Inbasekaran M, Woo EP (1998) Appl Phys Lett 73:3055
40. Hu Y, Zhang Y, Liang F, Wang L, Ma D, Jing X (2003) Synth Met 137:1123
41. Yang Z, Yang S, Zhang J (2007) J Phys Chem A 111:6354
42. Frisch MJ, Trucks GW, Schlegel HB, Scuseria GE, Robb MA, Cheeseman JR, Montgomery JAJ, Vreven T, Kudin KN, Burant JC, Millam JM, Iyengar SS, Tomasi J, Barone V, Mennucci B, Cossi M, Scalmani G, Rega N, Petersson GA, Nakatsuji H, Hada M, Ehara M, Toyota K, Fukuda R, Hasegawa J, Ishida M, Nakajima T, Honda Y, Kitao O, Nakai H, Klene M, Li X, Knox JE, Hratchian HP, Cross JB, Adamo C, Jaramillo J, Gomperts R, Stratmann RE, Yazyev O, Austin AJ, Cammi R, Pomelli C, Ochterski JW, Ayala PY, Morokuma K, Voth GA, Salvador P, Dannenberg JJ, Zakrzewski VG, Dapprich S, Daniels AD, Strain MC, Farkas O, Malick DK, Rabuck AD, Raghavachari K, Foresman JB, Ortiz JV, Cui Q, Baboul AG, Clifford S, Cioslowski J, Stefanov BB, Liu G, Liashenko A, Piskorz P, Komaromi I, Martin RL, Fox DJ, Keith T, Al-Laham MA, Peng CY, Nanayakkara A, Challacombe M, Gill PMW, Johnson B, Chen W, Wong MW, Gonzalez C, Pople JA (2004) Gaussian 03, revision C.02. Gaussian Inc, Wallingford
43. Lee C, Yang W, Parr RG (1988) Phys Rev B 37:785
44. Barone V, Cossi M (1998) J Phys Chem A 102:1995
45. Cornard J-P, Lapouge C (2006) J Phys Chem A 110:7159
46. Domingo LR, Picher MT, Zaragozá RJ (1998) J Org Chem 63:9183
47. Shukla MK, Leszczynski J (2005) Int J Quantum Chem 105:387
48. Halls MD, Schlegel HB (2001) Chem Mater 13:2632
49. Zhang J, Frenking G (2004) J Phys Chem A 108:10296
50. Zhang J, Frenking G (2004) Chem Phys Lett 394:120
51. Gahungu G, Zhang J (2005) J Mol Struct: Theochem 755:19
52. Gahungu G, Zhang J (2005) J Phys Chem B 109:17762
53. Gahungu G, Zhang J (2005) Chem Phys Lett 410:302
54. Hu B, Gahungu G, Zhang J (2007) J Phys Chem A 111:4965
55. Ahlrichs R, Bär M, Häser M, Horn H, Kälmel C (1989) Chem Phys Lett 162:165
56. Santos L, Vargas A, Moreno M, Manzano BR, Lluch JM, Douhal A (2004) J Phys Chem A 108:9331
57. Forés M, Duran M, Solà M, Adamowicz L (1999) J Phys Chem A 103:4413
58. Formosinho SJ, Arnaut LG (1993) J Photochem Photobiol A 75:21
59. Ormson SM, Brown RG, Vollmer F, Rettig W (1994) J Photochem Photobiol A 81:65
60. Le Gourrierec D, Ormson SM, Brown RG (1994) Prog React Kinet 19:221
61. Jena NR, Mishra PC (2005) J Phys Chem B 109:14205
62. Balamurali MM, Dogra SK (2002) J Photochem Photobiol A 154:81
63. Migani A, Bearpark MJ, Olivucci M, Robb MA (2007) J Am Chem Soc 129:3703
64. Yamazaki S, Domcke W (2008) J Phys Chem A 112:7090
65. Zhu X-M, Wang H-G, Zheng X, Phillips DL (2008) J Phys Chem B 112:15828
66. Kasha M, Heldt J, Gormin D (1995) J Phys Chem 99:7281
67. Sancho-García JC, Brédas J-L, Beljonne D, Cornil J, Msrtínez-Álvarez R, Hanack M, Poulsen L, Gierschner J, Mack HG, Egelhaaf HJ, Oelkrug D (2005) J Phys Chem B 109:4872
68. Strickler SJ, Berg RA (1962) J Chem Phys 37:81
69. Dreuw A, Fleming GR, Head-Gordon M (2003) J Phys Chem B 107:6500
70. Dreuw A, Head-Gordon M (2004) J Am Chem Soc 126:4007
71. Walker RC, Mercer IP, Gould IR, Klug DR (2006) J Comput Chem 28:478
72. Tozer DJ, Amos RD, Handy NC, Roos BO, Serrano-Andres L (1999) Mol Phys 97:859